Open Access

Catalysis Research

LIDSEN Publishing Inc.

Research Article

Ethanol Oxidation on Gold Nanowire Containing Oxygen Impurities: A Study by Ab Initio Molecular Dynamics Simulations

Otto V.M. Bueno [1], Miguel A. San-Miguel [2], Edison Z. da Silva [1 *]

1. Institute of Physics 'Gleb Wataghin' University of Campinas-Unicamp 13083-859 Campinas, SP, Brazil; E-Mails: ottovmb@ifi.unicamp.br; zacarias@ifi.unicamp.br
2. Department of Physical Chemistry, Institute of Chemistry University of Campinas-Unicamp P. O. Box 6154, 13083-970 Campinas, SP, Brazil; E-Mail: smiguel@unicamp.br

* **Correspondence:** Edison Z. da Silva; E-Mail: zacarias@ifi.unicamp.br

Academic Editors: Pavlos Pandis and Christos Argirusis

Special Issue: Nano-Sized Catalysts: Syntheses, Characterization, and Reactivities

Catalysis Research
2022, volume 2, issue 4
doi:10.21926/cr.2204043

Received: October 10, 2022
Accepted: December 05, 2022
Published: December 14, 2022

Abstract

Linear atomic chain (LAC) gold nanowires (Au-NWs) containing oxygen impurities are materials that could be used as supports to stimulate chemical reactions. Its peculiar structural characteristics, such as abnormal Au-Au bonds, make it interesting to explore the chemical reactions of this material at a theoretical level. This work investigated the chemical reaction of ethanol supported on Au-NW containing two oxygen impurities. Using *ab initio* molecular dynamics simulations, it was shown that the presence of oxygen impurity in the LAC conditions the minimum energy paths (MEP) that ethanol will follow in its chemical transformation. When the structure of the LAC contains two oxygen impurities, the formation of acetaldehyde and acetic acid as reaction products were observed. Specifically, the presence of two oxygen impurities in the LAC favors the migration of hydrogens of the -CH_2- and -OH groups of ethanol towards the LAC. In addition, it was observed that the formation of the C-O bond was favored, which implies an additional reaction intermediate that leads to a total of two different reaction paths in ethanol oxidation.

© 2022 by the author. This is an open access article distributed under the conditions of the Creative Commons by Attribution License, which permits unrestricted use, distribution, and reproduction in any medium or format, provided the original work is correctly cited.

Keywords
Ethanol oxidation; DFT; nanowires; *ab initio* molecular dynamics

1. Introduction

Low-dimensional materials are currently being intensely studied due to their inherent advantages as catalysts [1, 2]. All these materials, in particular, transition metals and carbon nanowires, are of interest due to their ability to promote chemical reactions of industrial interest as well as in other applications [3-6]. Our particular interest in this work focused on addressing chemical reactions in gold nanowires (NWs) containing single-atom thick structures in the form of linear atomic chains (LACs).

The manufacture of linear atomic chain gold NWs is feasible due to innovative techniques such as metallic jump-to-contact, mechanically controllable break-junction, electrochemical growth, electron beam punching, and molecular jump-to-contact [7]. These techniques allow the design of NWs with predefined lengths and thicknesses and facilitate the study of the properties of NWs with diverse morphological and structural characteristics. Takayanagi et al. [8] were one of the first to fabricate ultra-thin gold NWs with thicknesses ranging from 0.8 to 2.0 nm and lengths of 5 to 10 ns, using an ultrahigh vacuum transmission electron microscope (UHVTEM). Later, this author managed to manufacture LAC with a length of four gold atoms [9], showing that the NWs are easy to fabricate. However, despite its easy manufacture on a laboratory scale, its manufacture on an industrial scale remains impossible, limiting its use as catalytic material. It is expected that this inconvenience will be resolved in a short time to take advantage of the potential offered by the NWs, mainly with LACs.

From the first experimental [8-10] and theoretical studies [11-15] on linear atomic chain Au-NWs to recent studies [16, 17], it has been observed that the NWs can easily modify their chemical and/or structural nature in the presence of any type of contaminant [11, 13-15]. It is clear that these studies suggested that NWs could be interesting materials to stimulate and explore different types of chemical reactions, such as organic/inorganic molecules. For example, a pure LAC of four gold atoms in the presence of CO and O_2 molecules can easily form a LAC of four gold atoms with an oxygen atom in its structure (Au-Au-O-Au-Au) [18]. This mechanism suggests that the introduction of oxygen in the LAC is a common process that favors the formation of LAC with different amounts of oxygen. This is feasible since LACs with up to ten gold atoms with varying oxygen contaminants were observed [19]. Furthermore, other studies have also shown that the oxygen atom in the LAC helps to keep the linear atomic chain stable, since the oxygen atom acts as an anchor for gold atoms [15, 19], suggesting that the NWs with oxygen impurity in their structure are consolidated materials.

The formation of LACs with different amounts of gold and oxygen atoms in their structure has been experimentally observed on several occasions [16, 20-23]. This suggests that LACs with different lengths and oxygen content in their structure are common in nature, and their formation may be relatively frequent [18, 19]. With this in mind, we performed simulation studies of the interaction of gold NWs in a high vacuum with an organic molecule. In the simulation, we used the nanowire designed by Nascimento et al. [18] as a starting point (Figure 1A). Subsequently, we modified the NW by adding an oxygen atom in the LAC (Figure 1B), and finally, we added another

oxygen atom to the NW (Figure 1C). The NW with two oxygen atoms was the reference structure to start our reactivity study (Figure 1C).

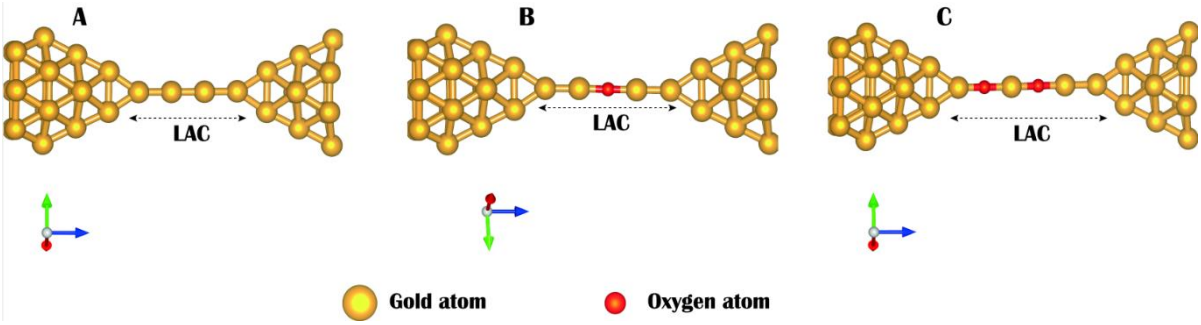

Figure 1 Linear atomic chain (LAC) gold nanowire with four gold atoms, with and without oxygen impurities in its structure. The model of pure NW [18] with four Au atoms LAC (A), with four Au atoms and one oxygen impurity atom LACs (B) and with two oxygen atoms (C).

Ethanol has been chosen as the organic molecule to interact with the LAC since its chemical reactions have been well established [24-26]. In particular, ethanol oxidation in heterogeneous catalysis has been well studied. For example, there are many reaction products of ethanol, including the formation of acetaldehyde [27], acetic acid [28], ethyl acetate [29], ethoxy [30], etc. All these products are formed mainly because the α-C-H, β-C-H, and O-H bonds are easily activated in the presence of transition metals [31, 32]. Even the activation of the C-C bond [33] also has been observed, which requires a lot of energy to break it in homogeneous catalysis. The activation of all bonds is the origin of the complex reaction behavior of ethanol.

This study used *ab initio* molecular dynamics coupled with well-tempered metadynamics [34] to understand the chemical reaction of ethanol supported on an NW containing two oxygen impurities in the LAC, under high vacuum conditions. Here, the reaction mechanism involving the activation of the β-C-H bond of the CH_2 group was stimulated [35, 36].

2. Methodology

All density functional theory calculations were performed using the CP2K program package [37, 38]. The electronic structure was calculated with the density functional theory (DFT) using the Perdew-Burke-Ernzerhof (PBE) functional [39, 40], which includes a reparameterization of the D3 Grimme density functional dispersion correction [41-43]. The QUICKSTEP module [44] was chosen for an efficient wave function optimization using the orbital transformation (OT) method [45], and to be able to combine Gaussians and Plane Waves (GPW) [46]. Wave functions were expanded in plane waves and Gaussians, using a cutoff of 650 Ry for plane waves and a real cutoff of 80 Ry for multiple grid mapping. The TZV2P-MOLOPT-GTH basis set was used for the C, H, and O atoms, and the DZVP-MOLOPT-SR-GTH basis set was used for the Au atom [47]. The valence electrons were used for Au($5d^{10}6s$), O($2s^2 2p^4$) and C($2s^2 2p^2$) atoms. Geodecker-Teter-Hutter pseudopotentials were adopted to model the core electron [48, 49].

The simulations were based on Born-Oppenheimer molecular dynamics (BOMD). In all simulations, the timestep and temperature were set to 0.5 fs and 300 K, respectively. The temperature was adjusted using Nosé-Hoover chain thermostats [50, 51]. Equilibration was

performed using a massive Nosé-Hoover chain thermostat, with the thermostat-time-constant set to τ = 10 fs. Subsequently, before data collection, the systems were simulated for 2 ps with a Nosé-Hoover chain global thermostat (thermostat-time-constant τ = 50 fs). Simulation cell sizes in X and Y were chosen to ensure space between the nanowires and to avoid interaction between their periodic images. The lengths of the simulation cells were defined as Lx = Ly = 20 Å. The movement of ethanol was constrained to the vicinity of the LAC, using an upper harmonic wall with a spring constant of k = 200 kcal mol^{-1} $Å^{-2}$. This prevents ethanol from exploring regions that are not of our interest, thus avoiding unnecessary computational costs.

Techniques such as metadynamics (including its variants) and potential energy surface (PES) scans were used to efficiently explore potential reaction paths, even those that could have high energy barriers. Without these techniques, it would be unfeasible to explore these reaction pathways successfully. Once the reaction path was achieved, techniques such as well-tempered metadynamics and nudged elastic band (NEB) were used to confirm and determine the minimum energy paths (MEP) of these reactions.

Specifically, molecular dynamics simulations were accelerated using the metadynamics technique [52] and the extended Lagrangian metadynamics technique [52]. In the metadynamics technique, the Gaussians were added every 30 fs. The height of the Gaussians was defined as 4.5 kcal/mol, and the width of the Gaussians was 0.9 Å. In the extended Lagrangian metadynamics technique, the parameters of the collective variables were defined with a virtual particle mass of 30.0 AMU, a coupling spring constant λ = 2.0 (lambda), and the temperature of the auxiliary variables was 300 K. In both techniques, reaction coordinates (collective variables) were defined using distances between atoms. The minimum energy path of all chemical reactions was quantified using the harmonic NEB method. Specifically, the climbing-image nudged elastic band (CI-NEB) [53, 54] was used. The spring constant value for NEB calculations was set to 0.02 au.

3. Results and Discussions

In this work, two reaction products were found during the oxidation of ethanol. The first observed was the formation of acetaldehyde, followed by acetic acid. The details of each reaction path are discussed below.

3.1 Acetaldehyde Formation

The entire reaction path is summarized in Figure 2, including the conformational changes induced by ethanol in the LAC before the chemical reaction occurs. Trajectory analysis shows that different relatively stable conformers are formed when ethanol interacts with the LAC (conformers 1, 2, and 3, Figure 2). Of the three conformers observed, trajectory analysis showed that conformer-3 is the conformation that causes the onset of the oxidation reaction. In addition, the energy cost required to go from any of conformers 1 and 2 to conformer 3 was analyzed. NEB-CI analysis showed that low energy barriers must be overcome to form conformer-3. For example, a barrier of ~0.10 eV needs to be overcome to go from conformer-1 to conformer-3, and an energy barrier of ~0.15 eV needs to be overcome to go from conformer-2 to conformer-3 (Figures 2A and 2B). The low energy barrier to evolve from any other conformers to conformer-3 suggests that the starting of the chemical reaction is not affected by conformational changes that could impede the oxidation reaction. The size of energy barriers is 3.9-5.8 times larger than the barrier defined by the thermal

fluctuations at 300 k (K_BT ~ 25.7 meV). It means that either conformer is easily formed at room temperature.

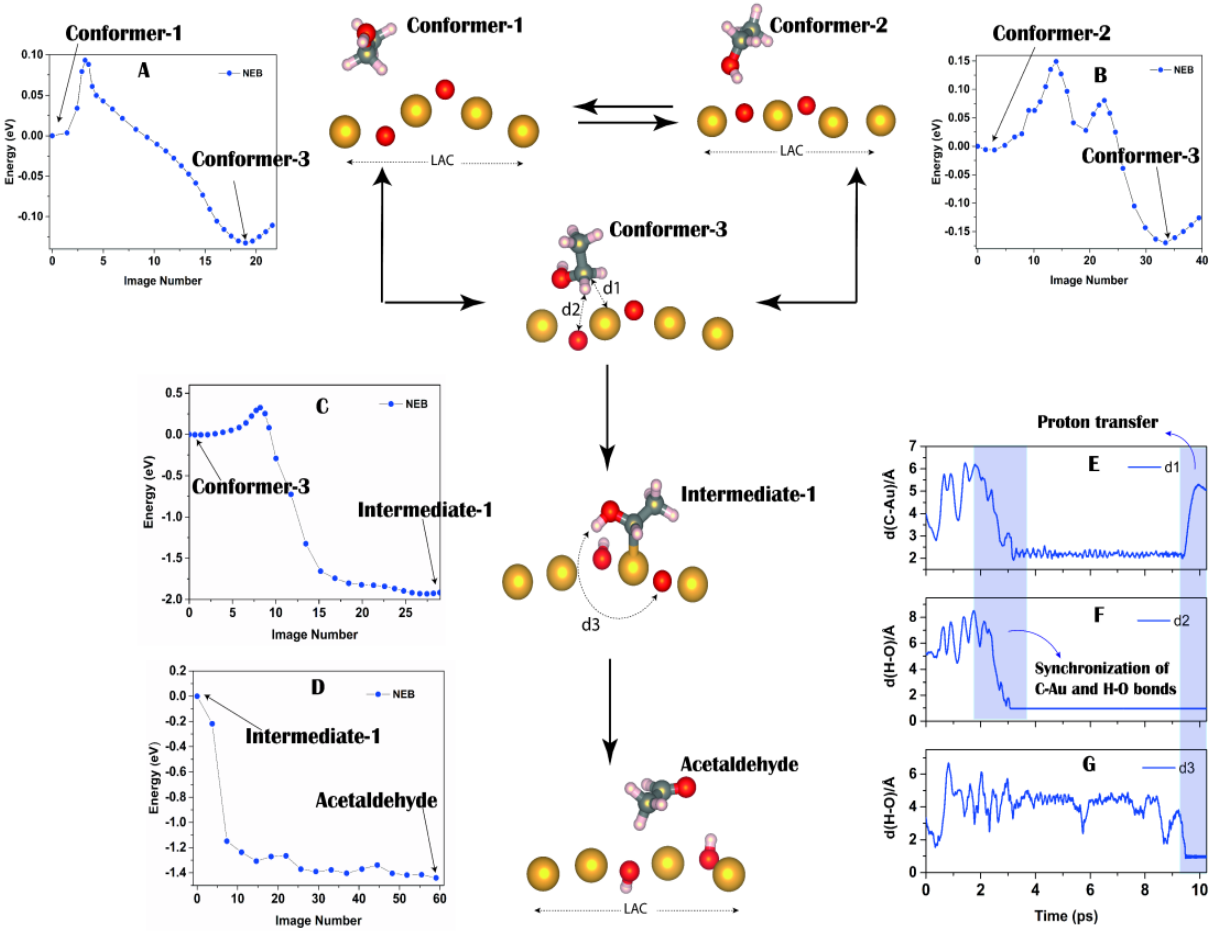

Figure 2 Oxidation reaction path of ethanol supported on Au-NW contaminated with two oxygen impurities. This figure summarizes the formation of acetaldehyde from ethanol. The tip of the NW is not plotted to show the parts of the LAC more clearly. (A) NEB analysis shows the minimum energy path for the conformational change from conformer-1 to conformer-3. (B) NEB analysis shows the minimum energy path for the conformational change from conformer-2 to conformer-3. (C) NEB results show the minimum energy path for the formation of intermediate-1 (the image of intermediate-1 was rotated for better visualization) from conformer-3. (D) NEB results show the minimum energy path for the formation of acetaldehyde from intermediate-1. (E, F, and G) Time evolution of the d1(C-Au), d2(-CH_2-O), and d3(-OH-O) distances along the simulation trajectory.

In the chemical reaction, we observe the formation of acetaldehyde in two reaction stages (Figures 2C and 2D). In the first stage, the formation of a stable chemical compound intermediate is observed, where a carbon atom bonds to a gold atom (intermediate-1, Figure 2). Specifically, this chemical compound intermediate was formed when the carbon atom of the —CH_2— group interacted with a gold atom of the LAC and synchronously transferred one of the hydrogens of the —CH_2— group to an oxygen atom of the LAC (Figures 2E and 2F). The synchronization confirmed that what happened was consolidated in only one stage. The synchronization of bond breaking and

bond formation was confirmed by analyzing the simulation trajectory of the distances d1 = $d_{(C-Au)}$ and d2 = $d_{(H-O)}$ (Figures 2E and 2F). The structure of the transition state (TS) in the minimum energy path from conformer-3 to intermediate-1 is shown in Supplementary material, Figure S1.

In the second stage, intermediate-1 was observed to remain stable for a long time. The simulation trajectory showed that it takes approximately 9 ps for the —OH proton of intermediate-1 to align with the other oxygen in the LAC. Once aligned, a proton transfer involving acetaldehyde formation can be observed. The proton transfer was indirectly confirmed by analyzing the simulation trajectory of the distance d3 = $d_{(H-O)}$ (Figure 2G). Also, the formation of acetaldehyde was confirmed by analyzing the distance d1 = $d_{(C-Au)}$ from ~9 ps of time evolution (Figure 2E).

Regarding the energy cost of the oxidation reaction, the results of the NEB-CI analysis showed that in the first stage (Figure 2C), only an activation energy barrier of ~0.34 eV needs to be crossed from conformer-3 to intermediate-1, that is, about 13 times the energy barrier defined by thermal fluctuation at room temperature (~25.7 meV). An energy barrier of that size suggests that the reaction is kinetically favorable and could occur quite easily. In the second stage (Figure 2D), the NEB results showed a negligible energy cost to form acetaldehyde, intermediate-1 readily gives way to acetaldehyde as long as proper orientation between the proton of intermediate-1 (—OH) and oxygen from the LAC occurs. As it is a proton transfer to an oxygen atom of the LAC, the energy cost is negligible in the second stage.

The initial and final stage of the process is summarized in the chemical equation below. The symbol ≡ denotes the tip of the NW.

$$CH_3CH_2OH + \equiv Au\text{-}O\text{-}Au\text{-}O\text{-}Au\text{-}Au\equiv \rightarrow CH_3CHO + \equiv Au\text{-}OH\text{-}Au\text{-}OH\text{-}Au\text{-}Au\equiv$$

On the other hand, the formation of acetaldehyde in pure LAC follows a different reaction path. For example, the second stage of this reaction occurs in an endothermic process that is very different from the one observed in the presence of oxygen atoms in the LAC (exothermic), see Supplementary material, Figure S2. This clearly shows that oxygen in the LAC drastically modifies the behavior of the ethanol reaction.

3.2 Acetic Acid Formation

Another reaction is also possible, where simulation trajectory analysis showed the formation of another intermediate (intermediate-2) from intermediate-1 (Figure 3). In this case, the C-Au bond consolidated during the formation of intermediate-1 is broken to form the C-O bond with one of the two oxygen atoms available in the LAC (LAC with two oxygen impurities). The temporal evolution of the distances d4 = $d_{(C-Au)}$ and d5 = $d_{(C-O)}$ confirms this behavior (Figure 3). Simulations show that this transformation requires about ~2.0 ps to occur. NEB-CI analysis shows that intermediate-2 is thermodynamically more stable than intermediate-1. Furthermore, the activation energy barrier to form intermediate-2 from intermediate-1 is ~0.22 eV, which is a low energy barrier that favors the formation of intermediate-2 easily. Once intermediate-2 is created, the energy required to return to intermediate-1 is very high, approximately 2.75 eV (Figure 3). Therefore, once the chemical compound intermediate-2 is formed, it will lead to the formation of a different reaction product. In the intermediate-2 configuration, the hydrogen trapped in the LAC oxygen (Au–OH–Au, Figure 3) can be released to interact with any LAC gold atoms (Au–H–Au) in a dynamic equilibrium process. This last configuration will be used to explore possible reaction paths in the formation of acetic acid.

The structure of the TS in the minimum energy path from intermediate-1 to intermediate-2 is shown in Supplementary material, Figure S3.

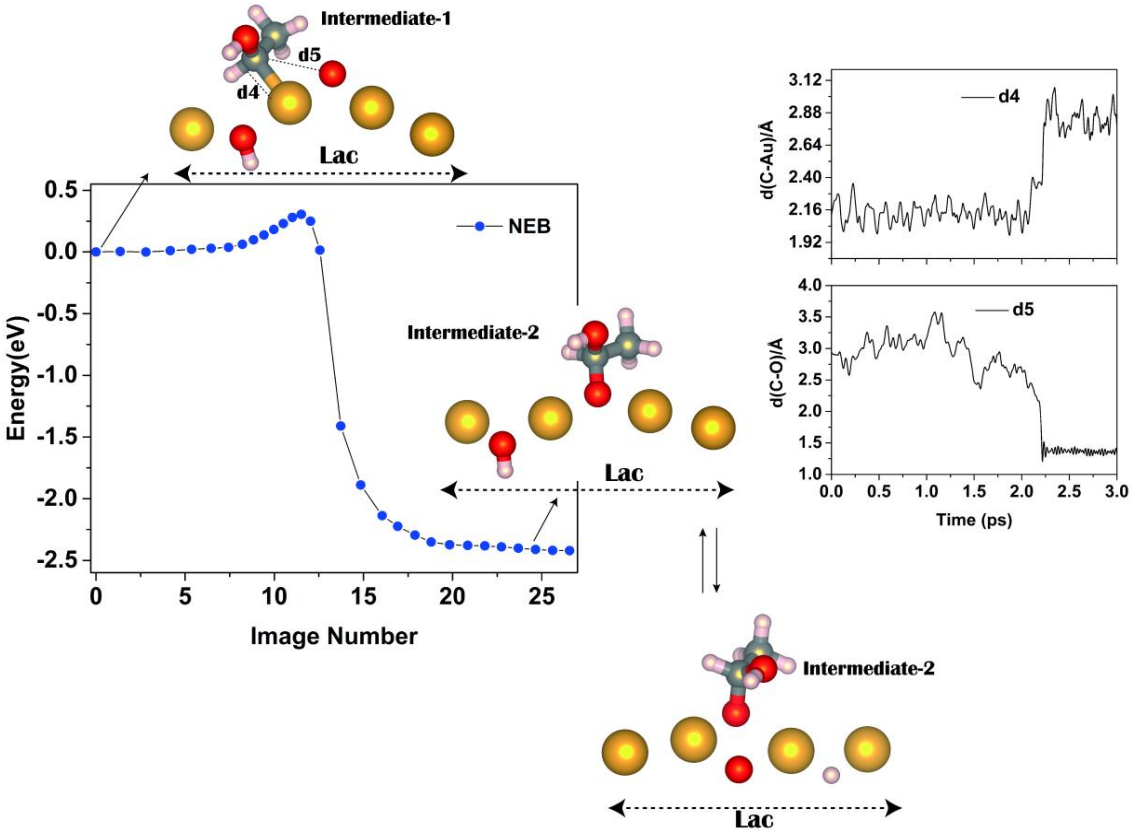

Figure 3 Analysis of the formation of intermediate-2 from intermediate-1. The NEB-CI result shows the minimum energy paths of this process. Indirectly, the temporal evolution of the distances d4 = $d_{(C\text{-}Au)}$ and d5 = $d_{(C\text{-}O)}$ shows the transformation from intermediate-1 to intermediate-2. Only the LAC part of the nanowires is shown in the figures for a clearer representation of the process.

The structure of intermediate-2 shows that the acetic acid molecule may be another reaction product. Intermediate-2 requires almost no loss of hydrogen from the —CH— group. Considering this possibility, a PES scan was performed to determine by which reaction path the migration of hydrogen —CH— would occur (Path 1, Path 2, and Path 3, Figure 4). Three possible different migration paths are presented where migration could occur: (i) Path 1, hydrogen from the —CH— group migrating to the gold atom (Figure 4A, A1, A2, and A3), (ii) Path 2, hydrogen from the —CH— group migrating to the oxygen (O1) of the intermediate-2 itself (Figure 4B, B1, B2, and B3 transposition reaction), and (iii) Path 3, hydrogen of the —CH— group migrating to oxygen (O2) from the LAC (Figure 4C, C1, C2, and C3).

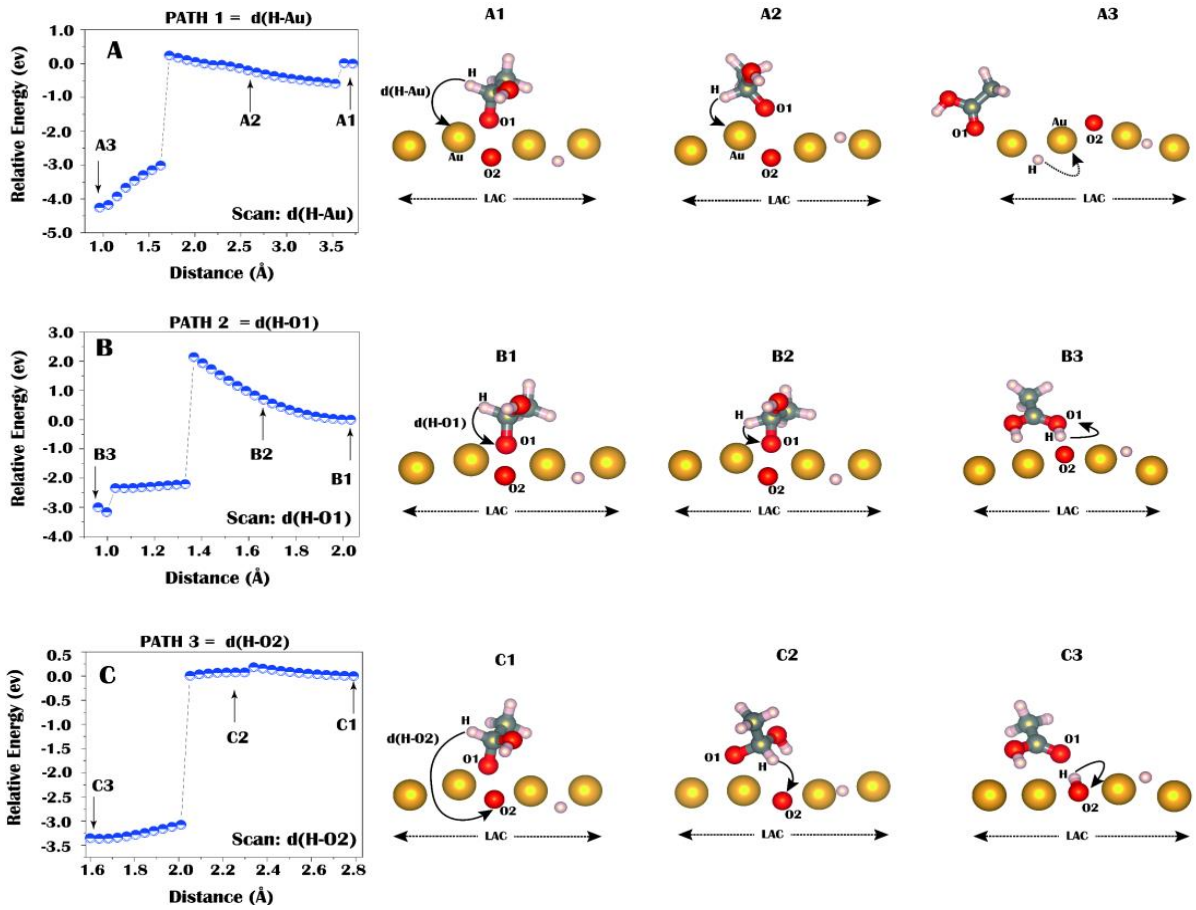

Figure 4 Migration of the hydrogen —CH— from intermediate-2 towards the LAC atoms studied using potential energy surface (PES) scan analysis. The migration of the hydrogen —CH— leads to the formation of acetic acid as the final product of the reaction. (A) The migration path of the hydrogen —CH— to a gold atom of the LAC. (B) The migration path of the hydrogen —CH— to the oxygen atom (O1) of the intermediate-2 itself, this path is known as a transposition reaction. (C) Migration path of the hydrogen —CH— to an oxygen atom (O2) of LAC.

It has been observed that the potential energy of the system decreases strongly when the migration of hydrogen —CH— takes any of the three possible reaction paths. In all three cases, the sharp drop in energy leads to a more stable configuration related to the formation of acetic acid. However, in each of these three cases, the energy barrier must be overcome to achieve this sharp drop in energy differs for each reaction path. In Path 1, when the hydrogen goes to the gold atom of the LAC from a distance of ~3.5 Å towards ~1.6 Å, it has to overcome an energy barrier of at least ~0.28 eV (Figure 4A). In Path 2, which involves a transposition migration, an energy barrier of at least ~2.0 eV has to be overcome (Figure 4B). In Path 3, when hydrogen goes to the oxygen atom of the LAC from ~2.8 Å to ~2.0 Å, an energy barrier of at least ~0.27 eV has to be overcome (Figure 4C). The Path 1 and Path 3 reaction pathways suggest that relatively low energy barriers must be overcome to form acetic acid. The barrier of Path 2 is ~7.4 times higher than Path 1 and Path 3 and is discarded. The formation of acetic acid could be given preferentially by Path 1 and Path 3. Therefore, only those possibilities were explored.

The reaction paths that lead to the acetic acid formation (Path 1 and Path 3) were selected with a low activation energy barrier, subsequently, *ab initio* molecular dynamics simulations coupled with well-tempered metadynamics were carried out to confirm these chemical reactions. For Path 1, the collective variables CV1 = $d_{C\text{-}H}$, and CV2 = $d_{Au\text{-}H}$ were chosen (Figure 5A), and for Path 3, the collective variables CV1 = $d_{C\text{-}H}$, and CV3 = $d_{O\text{-}H}$ were used (Figure 5B). Analysis of the free energy surface shows that the formation of acetic acid effectively occurs through two different reaction paths, both with low energy costs (in both cases, a ~0.28 eV barrier needs to be passed). This shows that the migration of the hydrogen —CH— from intermediate-2 occurs easily, both to the oxygen atom (O2) or the gold atom of the LAC. It is also noted that the free energy difference between intermediate-2 and acetic acid is approximately 0.6 eV. In other words, in the second stage of ethanol oxidation, the formation of acetic acid occurs in an exothermic process. The structure of the TS in the minimum energy path from intermediate-2 to the acetic acid is shown in Supplementary material, Figure S4.

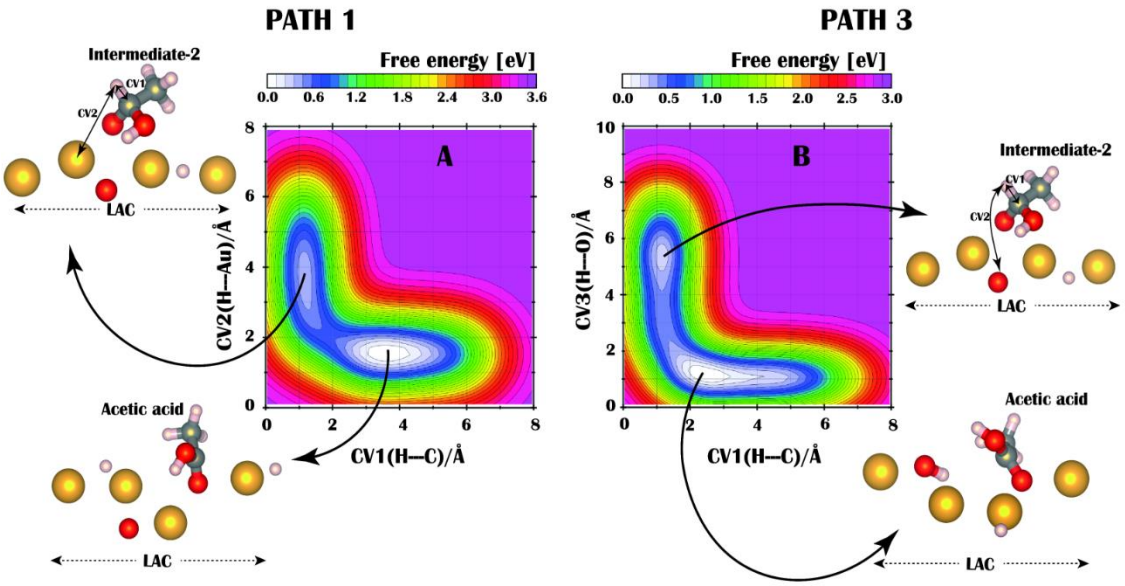

Figure 5 Free energy surface obtained in the formation of acetic acid from intermediate-2. The free energy surface was constructed considering the collective variables (or reaction coordinates) CV1 = $d_{C\text{-}H}$ and CV2 = $d_{Au\text{-}H}$ for reaction Path 1. For reaction Path 3, the collective variables CV1 = $d_{C\text{-}H}$ and CV3 = $d_{O\text{-}H}$ were used. (A) Path 1 shows the free energy surface when the hydrogen —CH— of intermediate-2 migrates to the gold atom. (B) Path 3 shows the free energy surface when the hydrogen —CH— of intermediate-2 migrates to the LAC oxygen atom.

The initial and final stages of the process are summarized in the chemical equation below. The symbol≡denotes the tip of the NW.

$$CH_3CH_2OH + \equiv Au\text{-}O\text{-}Au\text{-}O\text{-}Au\text{-}Au\equiv \rightarrow CH_3COOH + \equiv Au\text{-}OH\text{-}AuH\text{-}Au\text{-}Au\equiv$$

From the beginning of the reaction to the formation of the products, it was observed that the two oxygen impurities in the LAC play fundamental roles in the oxidation of ethanol. They favor the

migration of hydrogen from the molecules to the LAC and also the formation of C-O bonds, resulting in the formation of more than one reaction intermediate in the reaction path.

4. Conclusions

Ab initio molecular dynamics simulations, together with techniques such as metadynamics, PES scan, and NEB, have allowed the understanding of the complex behavior of the oxidation reaction of ethanol supported on a gold nanowire containing two oxygen impurities. Three types of conformers were found in the interaction between ethanol and the LAC, which have low energy barriers allowing conformer transformation by thermal fluctuations. The chemical reaction only starts when the system adopts the conformer-3 configuration in which the ethanol —CH_2— group is closest to the LAC.

Throughout the oxidation reaction of ethanol, the formation of two reaction products was observed: (i) acetaldehyde, and (ii) acetic acid.

4.1 Acetaldehyde

In the first instant, the formation of acetaldehyde was observed in two reaction stages. In the first stage, the formation of a stable intermediate chemical compound (intermediate-1) was observed, which remained stable for a long simulation time. In the second stage, this intermediate-1, through a proton transfer process, loses a proton to form acetaldehyde.

4.2 Acetic Acid

The formation of acetic acid is favored when intermediate-1 forms another thermodynamically more stable intermediate (intermediate-2). Through a proton transfer process, this second intermediate loses a proton (—CH—) through different reaction pathways to form acetic acid. Therefore, these results show that the presence of oxygen impurities in the LAC favors the formation of acetic acid.

In the formation of both reaction products, it can be seen that only in the first reaction stage considerable energy is required to stimulate the chemical reaction. The other stages involve proton transfer mechanisms and require much less energy than the first stage.

Acknowledgments

This work was carried out with the support of the São Paulo Research Foundation – FAPESP: 2013/07296-2, 2016/23891-6, 2017/26105-4 and 2020/11815-9. All calculations were performed at CCJDR-UNICAMP, Centro de Computação John David Rogers.

Author Contributions

All authors did all the research work for this study.

Competing Interests

The authors declare no conflict of interest.

Additional Materials

The following additional materials are uploaded at the page of this paper.

1. Supporting Information.

References

1. Tong X, Zhan X, Rawach D, Chen Z, Zhang G, Sun S. Low-dimensional catalysts for oxygen reduction reaction. Prog Nat Sci. 2020; 30: 787-795.
2. Xu B, Zhang Y, Li L, Shao Q, Huang X. Recent progress in low-dimensional palladium-based nanostructures for electrocatalysis and beyond. Coord Chem Rev. 2022; 459: 214388.
3. Abraham J, Arunima R, Nimitha KC, George SC, Thomas S. Chapter 3-One-dimensional (1D) nanomaterials: Nanorods and nanowires; nanoscale processing. In: Nanoscale processing. Amsterdam, the Netherlands: Elsevier; 2021. pp. 71-101.
4. Lada ZG, Chrissanthopoulos A, Perlepes SP, Andrikopoulos KS, Voyiatzis GA. Wet-chemistry assembly of one-dimensional nanowires: Switching characteristics of a known spin-crossover iron(ii) complex through Raman spectroscopy. Chem Commun. 2022; 58: 521-524.
5. Li T, Wu Y, Pei M. Screening of transition metal single-atom catalysts doped on γ-graphyne-like BN sheet for efficient nitrogen reduction reaction. J Alloys Compd. 2022; 908: 164675.
6. Parker M. Transition metal nanowires scale up. Nat Electron. 2021; 4: 12.
7. Lupu N. Electrodeposited nanowires and their applications. London, UK: IntechOpen; 2010.
8. Kondo Y, Takayanagi K. Gold nanobridge stabilized by surface structure. Phys Rev Lett. 1997; 79: 3455.
9. Ohnishi H, Kondo Y, Takayanagi K. Quantized conductance through individual rows of suspended gold atoms. Nature. 1998; 395: 780-783.
10. Rodrigues V, Ugarte D. Real-time imaging of atomistic process in one-atom-thick metal junctions. Phys Rev B. 2001; 63: 073405.
11. da Silva EZ, da Silva AJR, Fazzio A. How do gold nanowires break? Phys Rev Lett. 2001; 87: 256102.
12. Da Silva EZ, Novaes FD, da Silva AJR, Fazzio A. Theoretical study of the formation, evolution, and breaking of gold nanowires. Phys Rev B. 2004; 69: 115411.
13. Legoas SB, Galvão DS, Rodrigues V, Ugarte D. Origin of anomalously long interatomic distances in suspended gold chains. Phys Rev Lett. 2002; 88: 076105.
14. Novaes FD, da Silva AJR, da Silva EZ, Fazzio A. Effect of impurities in the large Au-Au distances in gold nanowires. Phys Rev Lett. 2003; 90: 036101.
15. Novaes FD, da Silva AJR, da Silva EZ, Fazzio A. Oxygen clamps in gold nanowires. Phys Rev Lett. 2006; 96: 016104.
16. Gonzalez-Garcia L, Maurer JHM, Reiser B, Kanelidis I, Kraus T. Ultrathin gold nanowires for transparent electronics: Breaking barriers. Procedia Eng. 2016; 141: 152-156.
17. Jiang X, Qiu X, Fu G, Sun J, Huang Z, Sun D, et al. Highly simple and rapid synthesis of ultrathin gold nanowires with (111)-dominant facets and enhanced electrocatalytic properties. J Mater Chem. 2018; 6: 17682-17687.
18. Nascimento APF, San-Miguel MA, Da Silva EZ. Unveiling the origin of oxygen atomic impurities in Au nanowires. Phys Rev B. 2014; 89: 085417.

19. Kizuka T. Atomic configuration and mechanical and electrical properties of stable gold wires of single-atom width. Phys Rev B. 2008; 77: 155401.
20. Smit RHM, Untiedt C, Rubio-Bollinger G, Segers RC, van Ruitenbeek JM. Observation of a parity oscillation in the conductance of atomic wires. Phys Rev Lett. 2003; 91: 076805.
21. Thijssen WHA, Marjenburgh D, Bremmer RH, van Ruitenbeek JM. Oxygen-enhanced atomic chain formation. Phys Rev Lett. 2006; 96: 026806.
22. Untiedt C, Yanson AI, Grande R, Rubio-Bollinger G, Agraït N, Vieira S, et al. Calibration of the length of a chain of single gold atoms. Phys Rev B. 2002; 66: 085418.
23. Yanson AI, Bollinger GR, van den Brom HE, Agraït N, van Ruitenbeek JM. Formation and manipulation of a metallic wire of single gold atoms. Nature. 1998; 395: 783-785.
24. Awasarkar PA, Sonsale AY, Chatterjee AK. Heterogeneous catalytic oxidation of ethanol: A new process for acetic acid. React Kinet Catal Lett. 1988; 36: 301-305.
25. Jacobse L, Vink SO, Wijngaarden S, Juurlink LBF. Heterogeneous catalytic oxidation of simple alcohols by transition metals. J Chem Educ. 2017; 94: 1285-1287.
26. Najafishirtari S, Friedel Ortega K, Douthwaite M, Pattisson S, Hutchings GJ, Bondue CJ, et al. A perspective on heterogeneous catalysts for the selective oxidation of alcohols. Chem Eur J. 2021; 27: 16809-16833.
27. Redina EA, Greish AA, Mishin IV, Kapustin GI, Tkachenko OP, Kirichenko OA, et al. Selective oxidation of ethanol to acetaldehyde over Au–Cu catalysts prepared by a redox method. Catal Today. 2015; 241: 246-254.
28. Xiang N, Xu P, Ran N, Ye T. Production of acetic acid from ethanol over CuCr catalysts via dehydrogenation-(aldehyde–water shift) reaction. RSC Adv. 2017; 7: 38586-38593.
29. Chen H, Dai Y, Jia X, Yu H, Yang Y. Highly selective gas-phase oxidation of ethanol to ethyl acetate over bi-functional Pd/zeolite catalysts. Green Chem. 2016; 18: 3048-3056.
30. Verma P, Vogiatzis KD, Planas N, Borycz J, Xiao DJ, Long JR, et al. Mechanism of oxidation of ethane to ethanol at iron(IV)–oxo sites in magnesium-diluted Fe_2(dobdc). J Am Chem Soc. 2015; 137: 5770-5781.
31. Behravesh E, Melander MM, Wärnå J, Salmi T, Honkala K, Murzin DY. Oxidative dehydrogenation of ethanol on gold: Combination of kinetic experiments and computation approach to unravel the reaction mechanism. J Catal. 2021; 394: 193-205.
32. Evans Jr EJ, Li H, Han S, Henkelman G, Mullins CB. Oxidative Cross-esterification and related pathways of co-adsorbed oxygen and ethanol on Pd–Au. ACS Catal. 2019; 9: 4516-4525.
33. Gong J, Mullins CB. Selective oxidation of ethanol to acetaldehyde on gold. J Am Chem Soc. 2008; 130: 16458-16459.
34. Barducci A, Bussi G, Parrinello M. Well-tempered metadynamics: A smoothly converging and tunable free-energy method. Phys Rev Lett. 2008; 100: 020603.
35. Donald WA, McKenzie CJ, O'Hair RAJ. C–H bond activation of methanol and ethanol by a high-spin FeIVO biomimetic complex. Angew Chem Int Ed. 2011; 50: 8379-8383.
36. Wu Z, Zhang M, Jiang H, Zhong CJ, Chen Y, Wang L. Competitive C–C and C–H bond scission in the ethanol oxidation reaction on Cu(100) and the effect of an alkaline environment. Phys Chem Chem Phys. 2017; 19: 15444-15453.
37. Hutter J, Iannuzzi M, Schiffmann F, VandeVondele J. cp2k: Atomistic simulations of condensed matter systems. Wiley Interdiscip Rev. 2014; 4: 15-25.

38. Kühne TD, Iannuzzi M, Ben MD, Rybkin VV, Seewald P, Stein F, et al. CP2K: An electronic structure and molecular dynamics software package-Quickstep: Efficient and accurate electronic structure calculations. J Chem Phys. 2020; 152: 194103.
39. Ernzerhof M, Scuseria GE. Assessment of the Perdew–Burke–Ernzerhof exchange-correlation functional. J Chem Phys. 1999; 110: 5029-5036.
40. Pedroza LS, da Silva AJR, Capelle K. Gradient-dependent density functionals of the Perdew-Burke-Ernzerhof type for atoms, molecules, and solids. Phys Rev B. 2009; 79: 201106.
41. Grimme S, Antony J, Ehrlich S, Krieg H. A consistent and accurate ab initio parametrization of density functional dispersion correction (DFT-D) for the 94 elements H-Pu. J Chem Phys. 2010; 132: 154104.
42. Grimme S, Ehrlich S, Goerigk L. Effect of the damping function in dispersion corrected density functional theory. J Comput Chem. 2011; 32: 1456-1465.
43. Smith DGA, Burns LA, Patkowski K, Sherrill CD. Revised damping parameters for the D3 dispersion correction to density functional theory. J Phys Chem Lett. 2016; 7: 2197-2203.
44. VandeVondele J, Krack M, Mohamed F, Parrinello M, Chassaing T, Hutter J. Quickstep: Fast and accurate density functional calculations using a mixed Gaussian and plane waves approach. Comput Phys Commun. 2005; 167: 103-128.
45. VandeVondele J, Hutter J. An efficient orbital transformation method for electronic structure calculations. J Chem Phys. 2003; 118: 4365-4369.
46. Lippert G, Hutter J, Parrinello M. A hybrid Gaussian and plane wave density functional scheme. Molecular Physics. 1997; 92: 477-488.
47. VandeVondele J, Hutter J. Gaussian basis sets for accurate calculations on molecular systems in gas and condensed phases. J Chem Phys. 2007; 127: 114105.
48. Goedecker S, Teter M, Hutter J. Separable dual-space Gaussian pseudopotentials. Phys Rev B. 1996; 54: 1703.
49. Hartwigsen C, Goedecker S, Hutter J. Relativistic separable dual-space Gaussian pseudopotentials from H to Rn. Phys Rev B. 1998; 58: 3641.
50. Martyna GJ, Klein ML, Tuckerman M. Nosé–Hoover chains: The canonical ensemble via continuous dynamics. J Chem Phys. 1992; 97: 2635-2643.
51. Nosé S. A unified formulation of the constant temperature molecular dynamics methods. J Chem Phys. 1984; 81: 511-519.
52. Iannuzzi M, Laio A, Parrinello M. Efficient exploration of reactive potential energy surfaces using Car-Parrinello molecular dynamics. Phys Rev Lett. 2003; 90: 238302.
53. Henkelman G, Jónsson H. Improved tangent estimate in the nudged elastic band method for finding minimum energy paths and saddle points. J Chem Phys. 2000; 113: 9978-9985.
54. Henkelman G, Uberuaga BP, Jónsson H. A climbing image nudged elastic band method for finding saddle points and minimum energy paths. J Chem Phys. 2000; 113: 9901-9904.

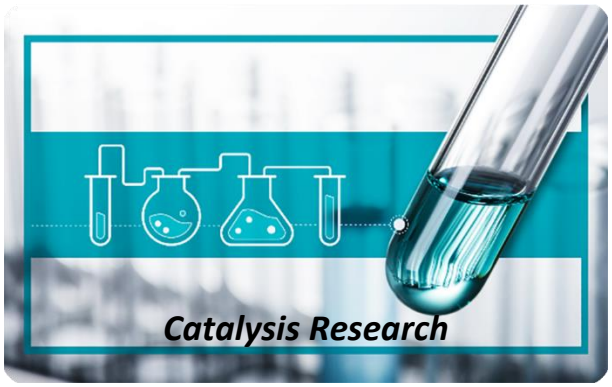

Enjoy *Catalysis Research* by:

1. Submitting a manuscript
2. Joining in volunteer reviewer bank
3. Joining Editorial Board
4. Guest editing a special issue

For more details, please visit:
http://www.lidsen.com/journals/cr